J|A|C|S
ARTICLES
Published on Web 12/30/2006

J-GFT NMR for Precise Measurement of Mutually Correlated Nuclear Spin−Spin Couplings

Hanudatta S. Atreya, Erwin Garcia, Yang Shen,[§] and Thomas Szyperski*

Contribution from The Northeast Structural Genomics Consortium and New York Consortium on Membrane Protein Structure, Department of Chemistry, State University of New York at Buffalo, Buffalo, New York 14260

Received September 15, 2006; E-mail: szypersk@chem.buffalo.edu

Abstract: G-matrix Fourier transform (GFT) NMR spectroscopy is presented for accurate and precise measurement of chemical shifts and nuclear spin−spin couplings correlated according to spin system. The new approach, named "*J*-GFT NMR", is based on a largely extended GFT NMR formalism and promises to have a broad impact on projection NMR spectroscopy. Specifically, constant-time *J*-GFT (6,2)D (HA−CA−CO)−N−HN was implemented for simultaneous measurement of five mutually correlated NMR parameters, that is, ^{15}N backbone chemical shifts and the four one-bond spin−spin couplings $^{13}C^{\alpha}-^{1}H^{\alpha}$, $^{13}C^{\alpha}-^{13}C'$, $^{15}N-^{13}C'$, and $^{15}N-^{1}H^{N}$. The experiment was applied for measuring residual dipolar couplings (RDCs) in an 8 kDa protein Z-domain aligned with Pf1 phages. Comparison with RDC values extracted from conventional NMR experiments reveals that RDCs are measured with high precision and accuracy, which is attributable to the facts that (i) the use of constant time evolution ensures that signals do not broaden whenever multiple RDCs are jointly measured in a single dimension and (ii) RDCs are multiply encoded in the multiplets arising from the joint sampling. This corresponds to measuring the couplings multiple times in a statistically independent manner. A key feature of *J*-GFT NMR, i.e., the correlation of couplings according to spin systems without reference to sequential resonance assignments, promises to be particularly valuable for rapid identification of backbone conformation and classification of protein fold families on the basis of statistical analysis of dipolar couplings.

1. Introduction

Modern NMR-based structural biology[1] relies on acquisition of multidimensional spectra. Conventional acquisition[2] of three-, four-, or higher dimensional NMR spectra is, however, limited by long minimal measurement times resulting from complete sampling of several indirect shift evolution periods. This key limitation of conventional NMR spectroscopy has been named the "NMR sampling problem".[3] G-matrix Fourier transform (GFT) projection NMR spectroscopy[4] can rapidly provide high-dimensional spectral information by joint sampling of $n \geq 2$ indirect chemical shift evolution periods, t_1, ..., t_j, ..., t_n, and thus represents one approach[3] to circumvent the NMR sampling problem. The joint sampling is repeated 2^n times so that time domain data sets are obtained which exhibit a transfer amplitude that is proportional to one of the 2^n permutations of products of cosine and sine modulations of the n jointly sampled shifts. Subsequent G-matrix Fourier transformation linearly combines these data sets. As a result, phase-sensitively detected peaks are located after Fourier transformation at positions corresponding to linear combinations of the jointly sampled shifts. Moreover, the peaks are edited into different sub-spectra according to the type of linear combination they encode, which ensures that the number of peaks per sub-spectrum is the same as in the high-dimensional parent spectrum.

Due to the high sampling speed, GFT NMR[4,5] allows one to avoid sampling limited NMR data acquisition,[3,6] and its efficiency for high-throughput protein structure determination[7] is documented by the fact that more than 20 protein structures with molecular weights ranging from about 10 to 23 kDa have so far been solved by the Northeast Structural Genomics Consortium and deposited in the Protein Data Bank.[8] Since 4D

[§] Current address: NIDDK, National Institutes of Health, Bethesda, MD 20892.

(1) (a) Rule, G. S.; Hitchens, T. K. *Fundamentals of Protein NMR Spectroscopy (Focus on Structural Biology)*, 1st ed.; Springer: Dordrecht, 2005. (b) Cavanagh, J.; Palmer, A. G.; Fairbrother, W. J.; Skelton, N. J.; Rance, M. *Protein NMR Spectroscopy: Principles and Practice*, 2nd ed.; Elsevier Science & Technology Books: Amsterdam, 2006; p 848.
(2) Ernst, R. R.; Bodenhausen, G.; Wokaun, A. *Principles of Nuclear Magnetic Resonance in One and Two Dimensions*; Oxford University Press: Oxford, UK, 1987.
(3) Atreya, H. S.; Szyperski, T. *Methods Enzymol.* **2005**, *394*, 78−108.
(4) Kim, S.; Szyperski, T. *J. Am. Chem. Soc.* **2003**, *125*, 1385−1393.
(5) (a) Kim, S.; Szyperski, T. *J. Biomol. NMR* **2004**, *28*, 117−130. (b) Atreya, H. S.; Szyperski, T. *Proc. Natl. Acad. Sci. U.S.A.* **2004**, *101*, 9642−9647. (c) Xia, Y. L.; Zhu, G.; Veeraraghavan, S.; Gao, X. L. *J. Biomol. NMR* **2004**, *29*, 467−476. (d) Atreya, H. S.; Eletsky, A.; Szyperski, T. *J. Am. Chem. Soc.* **2005**, *127*, 4554−4555. (e) Shen, Y.; Atreya, H. S.; Liu, G.; Szyperski, T. *J. Am. Chem. Soc.* **2005**, *127*, 9085−9099. (f) Eletsky, A.; Atreya, H. S.; Liu, G. H.; Szyperski, T. *J. Am. Chem. Soc.* **2005**, *127*, 14578−14579.
(6) Szyperski, T.; Yeh, D. C.; Sukumaran, D. K.; Moseley, H. N. B.; Montelione, G. T. *Proc. Natl. Acad. Sci. U.S.A.* **2002**, *99*, 8009−8014.
(7) Liu, G. H.; Shen, Y.; Atreya, H. S.; Parish, D.; Shao, Y.; Sukumaran, D. K.; Xiao, R.; Yee, A.; Lemak, A.; Bhattacharya, A.; Acton, T. A.; Arrowsmith, C. H.; Montelione, G. T.; Szyperski, T. *Proc. Natl. Acad. Sci. U.S.A.* **2005**, *102*, 10487−10492.
(8) Berman, H. M.; Westbrook, J.; Feng, Z.; Gilliland, G.; Bhat, T. N.; Weissig, H.; Shindyalov, I. N.; Bourne, P. E. *Nucleic Acids Res.* **2000**, *28*, 235−242.

10.1021/ja066586s CCC: $37.00

or 5D spectral information is encoded in the GFT NMR spectra recorded for resonance assignment,[5b,e,f,7] the completeness of resonance assignment is usually increased when compared with that of conventional 3D techniques. In turn, this impacts on the efficiency of (semi-)automated NOE assignment protocols.[9] GFT NMR is also employed in the context of a variety of other valuable projection NMR-based protocols, such as projection−reconstruction,[10] APSY,[11] and hi-fi NMR[12] (for recent reviews, see refs 3 and 13), which further emphasizes the central importance of GFT projection NMR spectroscopy for rapid acquisition of data in NMR-based structural biology.

A limitation of the currently used GFT NMR formalism arises from the fact that G-matrix transformation requires that the cosine and sine modulations in the 2^n data sets are *not* phase-shifted. The lack of methodology to apply a phase correction in the GFT dimension also imposes restrictions on the design of the radio frequency (rf) pulse sequences used to acquire the GFT data. Furthermore, this limitation impedes employment of GFT NMR for measurement of parameters other than chemical shifts whenever non-shifted sinusoidal modulations cannot be realized. In this publication, we present a generalized GFT NMR approach, which enables one to apply phase corrections in the GFT dimension or to employ GFT NMR for simultaneous and accurate measurement of chemical shifts and several spin−spin couplings, such as scalar or residual dipolar couplings.

It is well established that residual dipolar couplings (RDCs) are valuable NMR parameters yielding "orientational" constraints[14] to study biological macromolecules in solution. RDCs are used for (i) refining and validating NMR solution structures of single-domain proteins,[15] (ii) determining the relative orientation of domains in multidomain proteins and proteins in macromolecular complexes,[16] (iii) determining the tertiary fold of a protein when only sparse nuclear Overhauser enhancement (NOE)-derived distance constraint networks[17] can be obtained,[18] (iv) supporting the resonance assignment of proteins,[19] (v) identifying regular secondary structure elements,[20] and (vi) elucidating protein dynamics.[21] Since RDC-derived structural constraints can be obtained rapidly, they are also attractive for structural genomics.[22] A dense set of orientational constraints can be obtained if different *types* of RDCs are considered (for example, $^{13}C^{\alpha}-^{1}H^{\alpha}$, $^{15}N-^{1}H^{N}$, or $^{15}N-^{13}C'$ couplings). The tightness of the constraints used for structure calculations depends on (i) the absence of systematic errors that may arise from varying conditions present during NMR data acquisition for the different types of couplings, (ii) the proper identification and assessment of internal motional modes which partially average RDCs,[21] and (iii) evidently the precision of the RDC measurement *per se*.[15]

To minimize systematic errors, it is desirable to measure multiple RDCs simultaneously in a single experiment:[23] this ensures that all couplings are obtained with the same spectrometer setup and rf pulse duty cycle. In addition, it is advantageous to mutually *correlate* all RDCs and chemical shifts belonging to a given covalent moiety, thereby using the combined dispersion of several types of RDCs to break, for example, $^{15}N,^{1}H^{N}$ chemical shift degeneracy. Frequency labeling in a second indirect dimension to disperse signals may then be circumvented, and large sets of unambiguously grouped RDCs can be obtained from two-dimensional (2D) planes exhibiting high resolution in the indirect dimension. Notably, the shorter minimal measurement times of 2D versus 3D NMR approaches is advantageous when data need to be collected for slowly precipitating aligned protein samples: the different types of couplings, if measured separately, can turn out to be inconsistent with a single alignment tensor.[15]

Simultaneous measurement of RDCs has been implemented[23] using spin state separation/selection (IPAP,[25] S^3E/S^3CT,[26] α/β selection[27]) in the indirect dimension in conjunction with E.COSY-type[24] techniques, while TROSY[28] can been used to

(9) Güntert, P. *Prog. Nucl. Magn. Reson. Spectrosc.* **2003**, *43*, 105−125.
(10) (a) Kupce, E.; Freeman, R. *J. Am. Chem. Soc.* **2003**, *125*, 13958−13959. (b) Kupce, E.; Freeman, R. *J. Biomol. NMR* **2003**, *27*, 383−387. (c) Kupce, E.; Freeman, R. *J. Biomol. NMR* **2004**, *28*, 391−395. (d) Kupce, E.; Freeman, R. *J. Am. Chem. Soc.* **2004**, *126*, 6429−6440. (e) Coggins, B. E.; Venters, R. A.; Zhou, P. *J. Am. Chem. Soc.* **2004**, *126*, 1000−1001. (f) Venters, R. A.; Coggins, B. E.; Kojetin, D.; Cavanagh, J.; Zhou, P. *J. Am. Chem. Soc.* **2005**, *127*, 8785−8795. (g) Coggins, B. E.; Venters, R. A.; Zhou, P. *J. Am. Chem. Soc.* **2005**, *127*, 11562−11563. (h) Jiang, L.; Coggins, B. E.; Zhou, P. *J. Magn. Reson.* **2005**, *175*, 170−176.
(11) (a) Hiller, S.; Fiorito, F.; Wuthrich, K.; Wider, G. *Proc. Natl. Acad. Sci. U.S.A.* **2005**, *102*, 10876−10881. (b) Fiorito, F.; Hiller, S.; Wider, G.; Wüthrich, K. *J. Biomol. NMR* **2006**, *35*, 27−37.
(12) Eghbalnia, H. R.; Bahrami, A.; Tonelli, M.; Hallenga, K.; Markley, J. L. *J. Am. Chem. Soc.* **2005**, *127*, 12528−12536.
(13) Szyperski, T.; Atreya, H. S. *Magn. Reson. Chem.* **2006**, *44*, S51−S60.
(14) Prestegard, J. H. *Nat. Struct. Biol.* **1998**, *5*, 517−522.
(15) (a) Tolman, J. R.; Flanagan, J. M.; Kennedy, M. A.; Prestegard, J. H. *Proc. Natl. Acad. Sci. U.S.A.* **1995**, *92*, 9279−9283. (b) Tjandra, N.; Bax, A. *Science* **1997**, *278*, 1111−1114. Tolman, J. R. *Curr. Opin. Struc. Biol.* **2001**, *11*, 532−539. (c) Bax, A. *Protein Sci.* **2003**, *12*, 1−16. Lipsitz, R. S.; Tjandra, N. *Annu. Rev. Biophys. Biomol. Struct.* **2004**, *33*, 387−413. (d) Prestegard, J. H.; Bougault, C. M.; Kishore, A. I. *Chem. Rev.* **2004**, *104*, 3519−3540.
(16) (a) Dosset, P.; Hus, J. C.; Marion, D.; Blackledge, M. *J. Biomol. NMR* **2001**, *20*, 223−231. (b) Jain, N. U.; Wyckoff, T. J. O.; Raetz, C. R. H.; Prestegard, J. H. *J. Mol. Biol.* **2004**, *343*, 1379−1389.
(17) Wüthrich, K. *NMR of Proteins and Nucleic Acids*; Wiley: New York, 1986; pp 1−292.
(18) (a) Delaglio, F.; Kontaxis, G.; Bax, A. *J. Am. Chem. Soc.* **2000**, *122*, 2142−2143. (b) Mueller, G. A.; Choy, W. Y.; Yang, D. W.; Forman-Kay, J. D.; Venters, R. A.; Kay, L. E. *J. Mol. Biol.* **2000**, *300*, 197−212. (c) Fowler, C. A.; Tian, F.; Al-Hashimi, H. M.; Prestegard, J. H. *J. Mol. Biol.* **2000**, *304*, 447−460. (d) Hus, J. C.; Marion, D.; Blackledge, M. *J. Am. Chem. Soc.* **2001**, *123*, 1541−1542. (e) Andrec, M.; Du, P. C.; Levy, R. M. *J. Biomol. NMR* **2001**, *21*, 335−347. (f) Rohl, C. A.; Baker, D. *J. Am. Chem. Soc.* **2002**, *124*, 2723−2729. (g) Giesen, A. W.; Homans, S. W.; Brown, J. M. *J. Biomol. NMR* **2003**, *25*, 63−71.
(19) (a) Zweckstetter, M.; Bax, A. *J. Am. Chem. Soc.* **2001**, *123*, 9490−9491. (b) Tian, F.; Valafar, H.; Prestegard, J. H. *J. Am. Chem. Soc.* **2001**, *123*, 11791−11796. (c) Jung, Y. S.; Zweckstetter, M. *J. Biomol. NMR* **2004**, *30*, 25−35.
(20) (a) Mascioni, A.; Veglia, G. *J. Am. Chem. Soc.* **2003**, *125*, 12520−12526. (b) Walsh, J. D.; Wang, Y. *J. Magn. Reson.* **2005**, *174*, 152−162.
(21) (a) Tolman, J. R.; Flanagan, J. M.; Kennedy, M. A.; Prestegard, J. H. *Nat. Struct. Biol.* **1997**, *4*, 292−297. (b) Tolman, J. R.; Al-Hashimi, H. M.; Kay, L. E.; Prestegard, J. H. *J. Am. Chem. Soc.* **2001**, *123*, 1416−1424. (c) Peti, W.; Meiler, J.; Bruschweiler, R.; Griesinger, C. *J. Am. Chem. Soc.* **2002**, *124*, 5822−5833. (d) Meiler, J.; Peti, W.; Griesinger, C. *J. Am. Chem. Soc.* **2003**, *125*, 8072−8073. (e) Lakomek, N. A.; Carlomagno, T.; Becker, S.; Griesinger, C.; Meiler, J. *J. Biomol. NMR* **2006**, *34*, 101−115.
(22) (a) Montelione, G. T.; Zheng, D. Y.; Huang, Y. P. J.; Gunsalus, K. C.; Szyperski, T. *Nat. Struct. Biol.* **2000**, *7*, 982−985. (b) Valafar, H.; Prestegard, J. H. *Bioinformatics* **2003**, *19*, 1549−1555.
(23) (a) Wang, Y. X.; Marquardt, J. L.; Wingfield, P.; Stahl, S. J.; Lee-Huang, S.; Torchia, D.; Bax, A. *J. Am. Chem. Soc.* **1998**, *120*, 7385−7386. (b) de Alba, E.; Suzuki, M.; Tjandra, N. *J. Biomol. NMR* **2001**, *19*, 63−67. (c) Permi, P. *J. Biomol. NMR* **2003**, *27*, 341−349. (d) Bersch, B.; Rossy, E.; Coves, J.; Brutscher, B. *J. Biomol. NMR* **2003**, *27*, 57−67. (e) Ding, K. Y.; Gronenborn, A. M. *J. Am. Chem. Soc.* **2003**, *125*, 11504−11505. (f) Wienk, H. L. J.; Martinez, M. M.; Yalloway, G. N.; Schmidt, J. M.; Perez, C.; Rüterjans, H.; Löhr, F. *J. Biomol. NMR* **2003**, *25*, 133−145. (g) Hoshino, M.; Otting, G. *J. Magn. Reson.* **2004**, *171*, 270−276. (h) Vijayan, V.; Zweckstetter, M. *J. Magn. Reson.* **2005**, *174*, 245−253.
(24) (a) Griesinger, C.; Sørensen, O. W.; Ernst, R. R. *J. Chem. Phys.* **1986**, *85*, 6837−6852. (b) Montelione, G. T.; Wagner, G. *J. Am. Chem. Soc.* **1989**, *111*, 5474−5475.
(25) Ottiger, M.; Delaglio, F.; Bax, A. *J. Magn. Reson.* **1998**, *131*, 373−378.
(26) (a) Meissner, A.; Duus, J. O.; Sørensen, O. W. *J. Magn. Reson.* **1997**, *128*, 92−97. (b) Sørensen, M. D.; Meissner, A.; Sørensen, O. W. *J. Biomol. NMR* **1997**, *10*, 181−186.
(27) Andersson, P.; Weigelt, J.; Otting, G. *J. Biomol. NMR* **1998**, *12*, 435−441.
(28) Pervushin, K.; Riek, R.; Wider, G.; Wüthrich, K. *Proc. Natl. Acad. Sci. U.S.A.* **1997**, *94*, 12366−12371.

increase the precision of the measurements.[23c,f,g] These experiments suffer, however, from several drawbacks, which are exacerbated if multiple RDCs are measured simultaneously. (i) The creation of anti-phase magnetization for spin state separation requires an additional delay[25,27] and results in reduced sensitivity due to transverse relaxation. (ii) In-phase and anti-phase magnetization components relax differentially, so spectral artifacts arise from spin state selection/separation.[25] (iii) When multiple RDCs evolve simultaneously in a non-constant-time[1] fashion, the resulting signals are broadened since transverse relaxation rates add up,[29] which limits the precision of simultaneous RDC measurements significantly.

Taking advantage of the generalized GFT NMR formalism, we present here a constant-time (ct) G-matrix Fourier transform NMR experiment[4] which circumvents the drawbacks alluded to above for simultaneous and precise measurement of multiple correlated RDCs in proteins. Four one-bond couplings, namely, $^{13}C^{\alpha}-^{1}H^{\alpha}$, $^{13}C^{\alpha}-^{13}C'$, $^{15}N-^{13}C'$, and $^{15}N-^{1}H^{N}$, and ^{15}N and $^{1}H^{N}$ chemical shifts are correlated. The new experiment is named "*J*-GFT (6,2)D (HA−CA−CO)−N−HN", where each dash represents one of the measured one-bond spin−spin couplings while for nuclei in parentheses the chemical shifts are not measured.

2. Theory

2.1. Generalized GFT Projection NMR. Phase shifts of NMR signals arise either from improper settings of rf pulse phases or corresponding delays between rf pulses or from non-resonant effects of rf pulses.[1] In conventional multidimensional NMR, correction of such phase shifts can be accomplished in a straightforward manner. In contrast, chemical shifts are jointly sampled in GFT projection NMR, so phase errors of the individual shifts are "entangled". This leads to complex, partially disperse spectral line shapes as well as "cross-talk" between the edited sub-spectra. In the following, we develop a GFT projection NMR formalism that explicitly considers phase errors, thus representing an extension of the formalism previously introduced by Kim and Szyperski.[4]

In (*N*,*N*−*K*)D GFT NMR, *K*+1 indirect evolution periods can be jointly sampled in order to detect linear combinations of *K*+1 NMR parameters α_j ($0 \le j \le K$), which can be either chemical shifts or nuclear spin−spin couplings. This results in 2^K "basic" spectra, each containing a real part and an imaginary part arising from phase-sensitive detection of α_j. Quite generally, α_0 is chosen to be a well-dispersed chemical shift, around which the multiplets encoding the values for the other parameters α_j ($j \ge 1$) are centered. The 2^{K+1} transfer amplitudes are proportional to all possible products of $\sin(\alpha_j t)$ and $\cos(\alpha_j t)$ modulations, which can be written as a 2^{K+1}-dimensional vector arising from tensor product formation according to[4]

$$\mathbf{S}(K) = \begin{bmatrix} C_K \\ S_K \end{bmatrix} \otimes \ldots \otimes \begin{bmatrix} C_1 \\ S_1 \end{bmatrix} \otimes \begin{bmatrix} C_0 \\ S_0 \end{bmatrix} \tag{1}$$

where, for brevity, one defines $c_j := \cos(\alpha_j t)$ and $s_j := \sin(\alpha_j t)$ ($j = 0, \ldots, K$) and t represents the evolution time in the "GFT dimension". Multiplication of $\mathbf{S}(K)$ with the **G**-matrix according to

$$\mathbf{T}(K) = \mathbf{G}(K) \cdot \mathbf{S}(K) \tag{2}$$

yields a vector $\mathbf{T}(K)$ with elements that are proportional to the transfer amplitudes of the desired edited sub-spectra[4] in which linear combinations of the NMR parameters α_j are phase-sensitively detected.

Introducing that the sine and cosine modulations may be phase-shifted, with Φ_c and Φ_s, one obtains an analogous vector, $\mathbf{S}'(K)$, defined as

$$\mathbf{S}'(K) = \begin{bmatrix} C_K' \\ S_K' \end{bmatrix} \otimes \ldots \otimes \begin{bmatrix} C_0' \\ S_0' \end{bmatrix} \tag{3}$$

where

$$\begin{bmatrix} C_i' \\ S_i' \end{bmatrix} = \begin{bmatrix} \cos(\alpha_i t_i + \Phi_{ci}) \\ \sin(\alpha_i t_i + \Phi_{si}) \end{bmatrix} = \begin{bmatrix} \cos\Phi_{ci} & -\sin\Phi_{ci} \\ \sin\Phi_{si} & \cos\Phi_{si} \end{bmatrix} \begin{bmatrix} \cos(\alpha_i t_i) \\ \sin(\alpha_i t_i) \end{bmatrix} \tag{4}$$

Defining a phase matrix $\mathbf{P}_i$ as

$$\mathbf{P}_i = \begin{bmatrix} \cos\Phi_{ci} & -\sin\Phi_{ci} \\ \sin\Phi_{si} & \cos\Phi_{si} \end{bmatrix} = \begin{bmatrix} c\Phi_{ci} & -s\Phi_{ci} \\ s\Phi_{si} & c\Phi_{si} \end{bmatrix} \tag{5}$$

yields

$$\begin{bmatrix} C_i' \\ S_i' \end{bmatrix} = \mathbf{P}_i \cdot \begin{bmatrix} C_i \\ S_i \end{bmatrix} \tag{6}$$

and after inversion of the non-singular matrix $\mathbf{P}_i$, one obtains

$$\begin{bmatrix} C_i \\ S_i \end{bmatrix} = \mathbf{P}_i^{-1} \cdot \begin{bmatrix} C_i' \\ S_i' \end{bmatrix}$$

$$\text{with } \mathbf{P}_i^{-1} = \frac{1}{c\Phi_{ci}\, c\Phi_{si} + s\Phi_{ci}\, s\Phi_{si}} \begin{bmatrix} c\Phi_{si} & s\Phi_{ci} \\ -s\Phi_{si} & c\Phi_{ci} \end{bmatrix} \tag{7}$$

With eqs 5 and 6, $\mathbf{S}'(K)$ defined in eq 3 can be written as

$$\mathbf{S}'(K) = \left(\mathbf{P}_K \cdot \begin{bmatrix} C_K \\ S_K \end{bmatrix} \right) \otimes \ldots \otimes \left(\mathbf{P}_0 \cdot \begin{bmatrix} C_0 \\ S_0 \end{bmatrix} \right) \tag{8}$$

and the "phase-corrected" vector $\mathbf{S}(K)$ can be obtained from $\mathbf{S}'(K)$:

$$\mathbf{S}(K) = (\mathbf{P}_K \otimes \ldots \otimes \mathbf{P}_0)^{-1} \cdot \mathbf{S}'(K) \tag{9}$$

The subsequent G-matrix transformation according to eq 2 yields the desired phase-corrected edited sub-spectra encoding linear combinations of NMR parameters. These phases can be inferred from knowledge of the particular implementation of the rf pulse scheme, or they can be derived by using a "bottom-up" approach analogous to the procedure previously introduced for unambiguous identification of chemical shift multiplet components.[4,30]

To illustrate the principles of generalized GFT NMR, cross sections taken along the GFT dimension of the four basic sub-spectra of a hypothetical (*N*,*N*−2)D experiment were calculated

(29) Kontaxis, G.; Clore, G. M.; Bax, A. *J. Magn. Reson.* **2000**, *143*, 184−196.

(30) Central peak spectra up to *K*th order can be recorded by successively omitting parameters from the joint sampling. The *K*th-order central peak spectrum measures solely a chemical shift, α_0, and the associated phases, Φ_{c0}, can be conventionally determined. Having those, the phases Φ_{c1} and Φ_{c1} can be adjusted in the (*K*−1)th central peak spectra, which in turn allows one to adjust the phases Φ_{c1} and Φ_{c2} in the (*K*−2)th central peak spectra. Such consecutive determination of phases can be continued until Φ_{cK} and Φ_{cK} are obtained from the basic spectra.

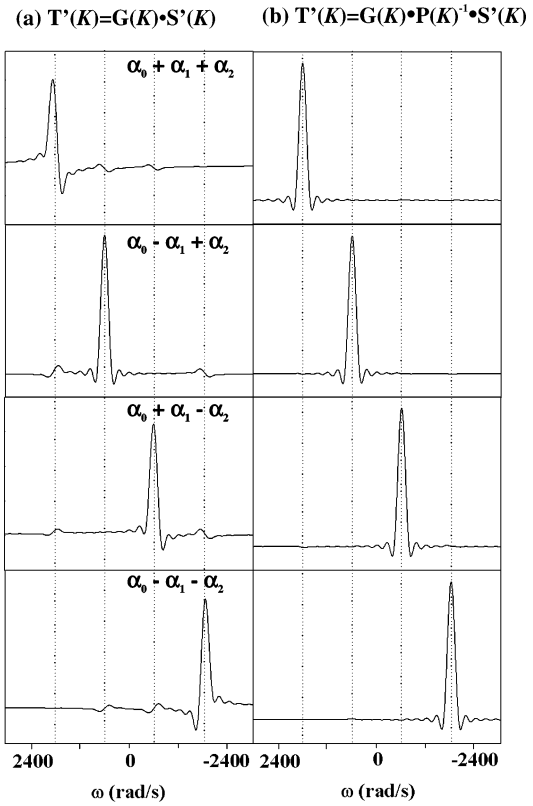

Figure 1. (a) Cross sections taken along the GFT dimension of a hypothetical constant-time (*N*,*N*−2)D GFT NMR experiment calculated with eq 2 and assuming that three NMR parameters, $\alpha_0/2\pi = 0$ Hz, $\alpha_1/2\pi =$ 100 Hz, and $\alpha_2/2\pi = 200$ Hz, are jointly sampled with phase sifts of, respectively, $\Phi_{c0} = 5°$, $\Phi_{c1} = 10°$, and $\Phi_{c2} = 15°$ for the cosine and $\Phi_{s0} = 7.5°$, $\Phi_{s1} = 15.0°$, and $\Phi_{s2} = 22.5°$ for the sine modulations of the time domain data (maximum evolution time, 25 ms). The phase matrix (eq 9) is given in the Supporting Information. After the G-matrix transformation, but before Fourier transformation, time domain data were multiplied with a cosine window function. The "cross-talk" between the sub-spectra (see text) resulting from the phase shifts is apparent by following the vertical dotted lines. (b) Same cross sections as in (a), except that eq 9 was used to ensure proper phase correction prior to GFT. This results in purely absorptive line shapes while cross-talk between the sub-spectra is eliminated.

(Figure 1). Three NMR parameters were assumed to be jointly sampled with different phase shifts for cosine and sine modulations. The apparent phase distortions as well as the "cross-talk" between the sub-spectra arising from the phase shifts (Figure 1a) are apparent but can be removed by employing a phase correction according to eq 9 prior to GFT (Figure 1b).

2.2. Theory of *J*-GFT NMR for Accurate Measurement of Spin−Spin Couplings. Sinusoidal modulations of the transfer amplitude by evolution of a chemical shift (Ω_S) and/or a spin−spin coupling $K = J + D$ (*J* and *D* represent, respectively, scalar and residual dipolar couplings) can be accomplished during a polarization transfer delay. In *J*-GFT NMR, phase-sensitive detection of the shift(s) is accomplished by use of STATES/TPPI.[1] For phase-sensitive detection of the coupling *K*, subspectra are acquired in which the transfer amplitude is either cosine- or sine-modulated with *K*. As a result, the coupling evolution can formally be treated like a chemical shift, and several couplings can be jointly sampled, as was introduced for chemical shifts in the framework of GFT NMR spectroscopy.[4] The cosine/sine modulations with *K* depend on tuning of a delay τ, affecting the transfer amplitude according to $\sin[\pi^*K(\tau + \kappa^*t)]$ (κ denotes a scaling factor;[4] appropriate rf pulse modules are discussed in the next section). For $\tau = 0$, one obtains, independent of the particular value of *K*, a sine modulation with $\sin(\pi^*\kappa K^*t)$. In contrast, $\tau = {}^1/_2\, K^{ave}$, where K^{ave} represents the average of the couplings in the system under consideration, yields a cosine modulation according to $\sin[\pi^*K(\tau + \kappa^*t)] = \cos(\pi^*\kappa K^*t)$.

If $K \neq K^{ave}$, a phase shift of Φ_c results according to

$$\sin(\pi^*K(\tau + \kappa^*t)) \rightarrow \cos(\pi^*\kappa K^*t + \pi/2^*(K - K^{ave})/K^{ave}) \rightarrow \cos(\pi^*\kappa K^*t + \Phi_c) \quad (10)$$

where * denotes a multiplication. In experiments measuring several couplings, each coupling of type *i* gives rise to a cosine modulation which is shifted by Φ_{ci}. Since

$$\cos[\pi^*\kappa_i K_i^*t + \Phi_{ci}] = \cos(\pi^*\kappa_i K_i^*t)\cos(\Phi_{ci}) - \sin(\pi^*\kappa_i K_i^*t)\sin(\Phi_{ci}) \quad (11)$$

the phase shifts Φ_{ci} introduce dispersive components into the line shapes and shift peak maxima. This impedes accurate measurement of the couplings.[31] Figure 2 illustrates the effect of a 30° phase shift of the cosine-modulated transfer amplitude on a G-matrix transformation. Taken together, the *spin-system-specific* phase shifts of the cosine-modulated data sets represent the major challenge for implementing *J*-GFT NMR experiments.

Spin-System-Specific Phase Correction. To cope with the phase shifts of the cosine-modulated data sets, a *spin-system-specific* phase correction can be applied according to eq 9. Using eqs 4, 5, and 10, the phase matrix **P** of eq 5 is given by

$$\mathbf{P}_i = \begin{bmatrix} c\Phi_{ci} & -s\Phi_{ci} \\ 0 & 1 \end{bmatrix} \quad (12)$$

Since the phase shift depends on the actual value of the spin−spin coupling, a different correction is required for each multiplet detected along the GFT dimension. Moreover, since the couplings are initially not known, an iterative protocol is required. The couplings are measured approximately in spectra processed without phase correction (this is equivalent to considering a 0^0 phase correction matrix, $\mathbf{P}^0$, equal to the unity matrix). The values obtained in this way are used to compute the phase matrix for each multiplet (first iteration phase matrix, $\mathbf{P}_i^1$). Improved values for the couplings can subsequently be obtained in the phase-corrected spectra. This can be repeated until the measured couplings remain invariant between cycles (i.e., $|\mathbf{P}_i^r - \mathbf{P}_i^{r+1}| \approx 0$, where *r* indicates the iteration number). In practice, a single iteration is sufficient, as verified using experimental data (see Results and Discussion).

Mirrored Time Domain Sampling. As an alternative to such iterative phase correction, we show in the following that recording of an additional data set with a transfer amplitude proportional to $\sin[\pi K_i(\tau - \kappa_i^*t)] = \cos(\pi^*\kappa_i K_i^*t - \Phi_{ci})$ enables one to eliminate dispersive signal components irrespective of the value of K_i. In analogy to eq 11, we have

$$\cos(\pi^*\kappa_i K_i^*t - \Phi_{ci}) = \cos(\pi^*\kappa_i K_i^*t)\cos(\Phi_{ci}) + \sin(\pi^*\kappa_i K_i^*t)\sin(\Phi_{ci}) \quad (13)$$

so that the sum of eqs 11 and 13 is given by

(31) Brutscher, B. *J. Magn. Reson.* **2001**, *151*, 332−338.

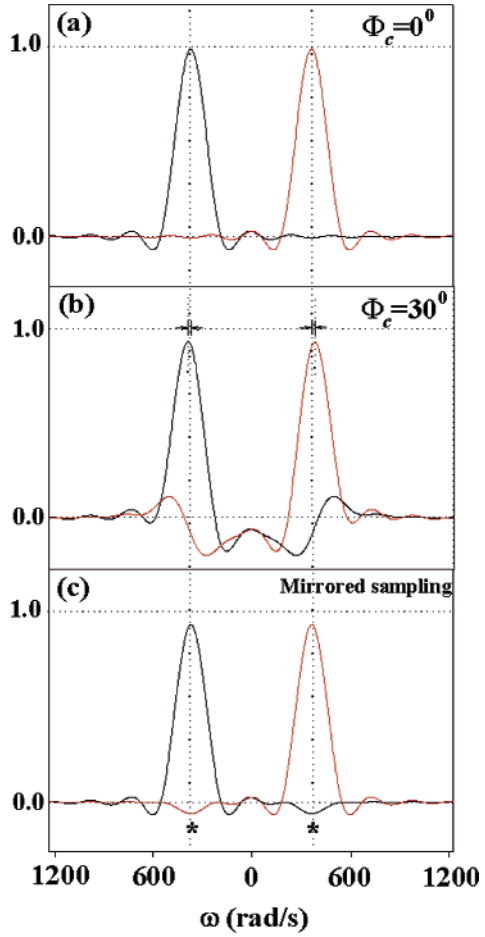

Figure 2. (a) Upfield (red) and low-field (black) signals of a GFT NMR doublet encoding in the signal splitting an experimental parameter with a value of 60 Hz (K = 60 Hz; K^{ave} = 90 Hz; e.g., a one-bond $^{15}N-^{1}H^{N}$ spin−spin coupling). To facilitate visual comparison, the maximum of peak intensity in (a) is shown by horizontal dashed lines in all spectra and the positions of the peak maxima are indicated by dashed vertical lines. (b) Same as is (a), except that the cosine modulation is shifted in phase by Φ_c = 30° (see eqs 10 and 11). Dark lines with arrow marks indicate the changes in the peak maxima due to the phase shifts. (c) Suppression of phase errors by employment of mirrored sampling of the time domain (see text). The asterisks indicates minor "quadrature artifacts" remaining at only ~6% of the peak height. Those arise from different amplitudes of the cosine and sine modulations (eq 14).

$$\cos(\pi^*\kappa_i K_i^*t + \Phi_{ci}) + \cos(\pi^*\kappa_i K_i^*t - \Phi_{ci}) = 2\cos(\pi^*\kappa_i K_i^*t)\cos(\Phi_{ci}) \quad (14)$$

Since this corresponds to sampling the time domain in the reverse direction, we named this approach "mirrored time domain sampling". The phase shift thus *solely* affects the amplitude of the cosine-modulated signal while the phase shift is eliminated. Importantly, one has for $(K_i - K_i^{ave})/K_i^{ave} < 0.3$ that $\cos(\Phi_{ci}) > 0.9$ ($\Phi_{ci} = \pi/2^*(K_i - K_i^{ave})/K_i^{ave} = 30°$); i.e., phase shifts up to 30° hardly yield detectable "quadrature images" as a result of the transfer amplitude being different for sine- and cosine-modulated data sets (Figure 2c). Note that such mirrored time domain sampling can be equally applied for correcting phase-shifted sine-modulated signals, since

$$\sin(\pi^*\kappa_i K_i^*t + \Phi_{si}) + \sin(\pi^*\kappa_i K_i^*t - \Phi_{si}) = 2\sin(\pi^*\kappa_i K_i^*t)\cos(\Phi_{si}) \quad (15)$$

Importantly, mirrored sampling of time domain data for more than one coupling requires an extension of the G-matrix formalism. This is because products of modulations arising from "forward" and "reverse" sampling of different couplings are formed. For brevity, we define $c_{1j} = \cos(\pi^*\kappa_j K_j^*t + \Phi_{cj})$, $c_{2j} = \cos(\pi^*\kappa_j K_j^*t - \Phi_{cj})$, $s_{1j} = \sin(\pi^*\kappa_j K_j^*t + \Phi_{sj})$, and $s_{2j} = \sin(\pi^*\kappa_j K_j^*t - \Phi_{sj})$. Since the cosine and sine modulations shall be added up to eliminate the phase shift, one has for $\cos(\Phi_{cj}) \approx 1$ and $\cos(\Phi_{sj}) \approx 1$,

$$e^{i\alpha_j} = (c_{1j} + c_{2j}) + i\cdot(s_{1j} + s_{2j}) = [1\ \ 1\ \ i\ \ i\,]\begin{bmatrix} c_{1j} \\ c_{2j} \\ s_{1j} \\ s_{2j} \end{bmatrix} \quad (16)$$

Considering that two jointly sampled parameters require mirrored time domain sampling, we obtain[4] for the phase-sensitive detection of sum and difference of two couplings K_1 and K_2

$$\begin{bmatrix} e^{i\alpha_1} \\ e^{-i\alpha_1} \end{bmatrix} \otimes e^{i\alpha_0} = \left[\begin{bmatrix} 1 & 1 & i & i \\ 1 & 1 & -i & -i \end{bmatrix} \otimes [1\ \ 1\ \ i\ \ i\,]\right] \cdot \left[\begin{bmatrix} c_{11} \\ c_{21} \\ s_{11} \\ s_{21} \end{bmatrix} \otimes \begin{bmatrix} c_{10} \\ c_{20} \\ s_{10} \\ s_{20} \end{bmatrix}\right] \quad (17)$$

In general, if M and N parameters require, respectively, mirrored and non-mirrored time domain sampling, one obtains for the G-matrix

$$\mathbf{G}(M,N) = \mathbf{G}^{mirrored}(M) \otimes \mathbf{G}(N) \quad (18)$$

where $\mathbf{G}(N)$ was described previously[4] and $\mathbf{G}^{mirrored}(M)$ is given by

$$\mathbf{G}^{mirrored}(M) = \mathbf{G}_M^{\ mirrored} \otimes \ldots \otimes \mathbf{G}_1^{\ mirrored} \quad (19)$$

with

$$\mathbf{G}_i^{\ mirrored} = \begin{bmatrix} 1 & 1 & i & i \\ 1 & 1 & -i & -i \end{bmatrix}$$

Subsequent multiplication of the time domain signal $\mathbf{S}(K)$, as defined in eq 1, according to

$$\mathbf{T}(K) = \mathbf{G}(M,N)\cdot\mathbf{S}(K) \quad (20)$$

yields the desired vector $\mathbf{T}(K)$, which represents the edited subspectra devoid of dispersive signal components.

2.3. Radio Frequency Pulse Modules for *J*-GFT NMR. Heteronuclear NMR experiments rely on INEPT-like polarization transfers, and the associated delays can be used for constant-time (ct) frequency labeling. In generalized ct *J*-GFT NMR, one may consider a multitude of different combinations of chemical shifts and spin−spin couplings for joint sampling. Following basic rules of the product−operator formalism,[2] we survey here rf pulse modules for phase-sensitive ct sampling of shifts and couplings. Several of those modules can be incorporated in order to jointly sample several NMR parameters. Considering scaling factors denoted as κ for the evolution of the respective NMR parameters, Figure 3a−c illustrates the modules designed for use of a single ct delay serving for magnetization transfer of (a) one coupling, (b) one coupling along with one chemical shift, and (c) two couplings along with

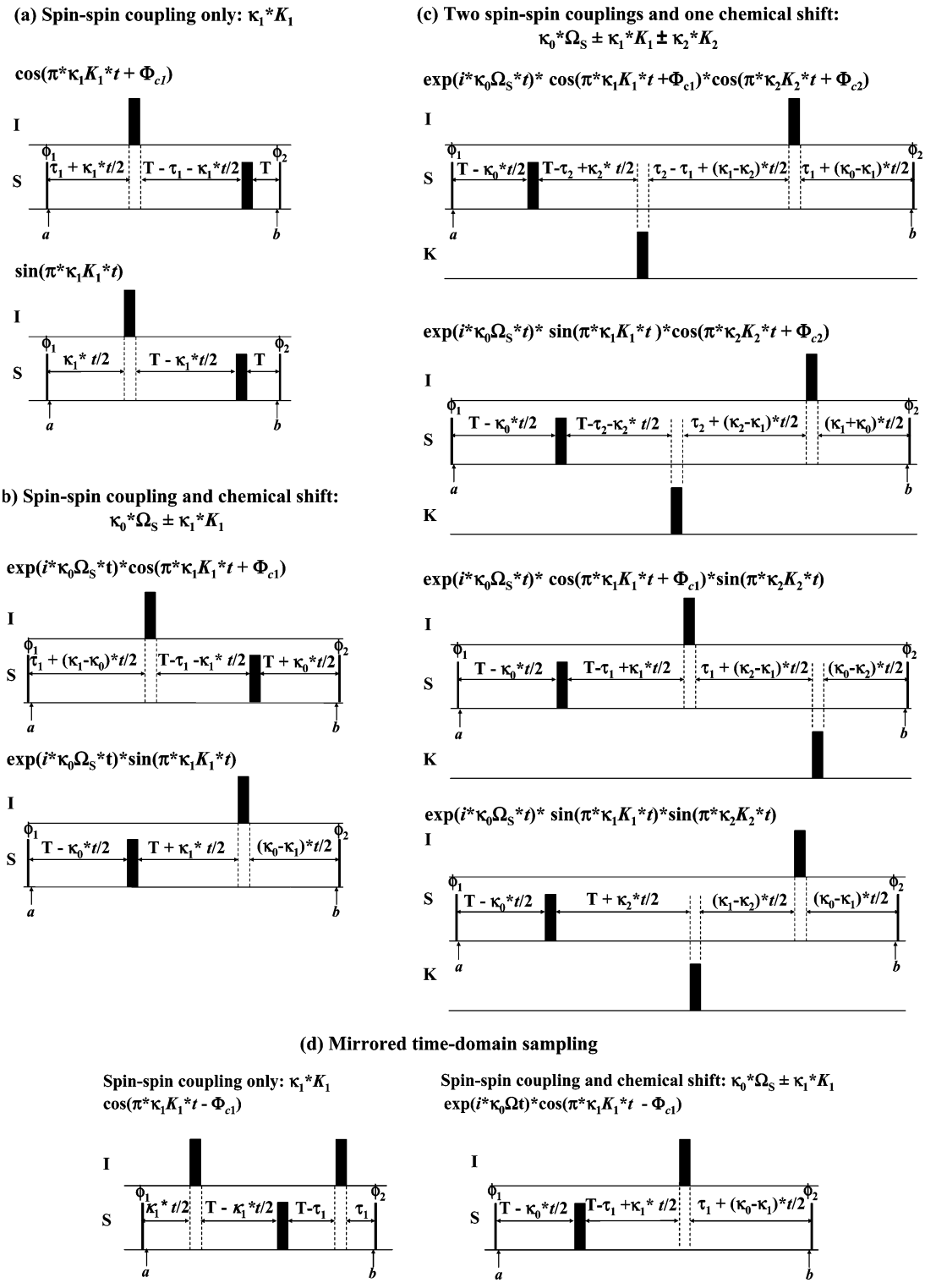

Figure 3. Radio frequency pulse modules which may serve as building blocks in *J*-GFT NMR experiments for detecting cosine and sine modulations of the transfer amplitude with chemical shifts (Ω_S) and/or spin−spin couplings. Rectangular 90° and 180° pulses are indicated by thin and thick vertical bars, respectively. The scaling factors for chemical shift and coupling evolution(s) are denoted as κ_0, κ_1, and κ_2, respectively. K_i^{ave} represents an average spin−spin coupling constant between spins I and S ($i = 1$), or between spins S and K ($i = 2$), in the system under consideration that is used to tune the delays τ_i. If $\tau_i = {}^1/_2\, K_i^{ave}$, the phase shift of the cosine-modulated signal is given by $\Phi_{ci} = \pi/2*(K_i - K_i^{ave})/K_i^{ave}$. T represents a constant-time delay for shift and coupling evolution. Cosine/sine modulation of Ω_S is accomplished by appropriately setting the phases, ϕ_1 and ϕ_2. For the spin state of *S* along *z* after the final 90° rf pulse required for detectable magnetization, $\phi_1 = \phi_2 = 0°,90°$ in (a) and (b), and $\phi_1 = 0°,90°$ and $\phi_2 = \phi_1 + 90°$ in (d). Note that for particular rf pulse scheme implementations, ϕ_1 and ϕ_2 will depend on the actual polarization transfer pathway. The product operator terms corresponding to the magnetization desired at time points indicated as ***a*** and ***b*** are listed in Table S1 of the Supporting information. Measurement of (a) a spin−spin coupling K_1 only, (b) a chemical shift Ω_S and a spin−spin coupling K_1 (for scaling factors $\kappa_0 \neq \kappa_1$, an alternative scheme can be used as shown in Figure S1 of the Supporting Information), (c) a chemical shift Ω_S and two spin−spin couplings, K_1 and K_2, and (d) mirrored time domain sampling scheme for (a) and (b).

one chemical shift. Figure 3d shows the modules that have to be incorporated in order to implement, respectively, mirrored sampling of an individual coupling and a coupling along with a chemical shift. Several of those modules can be incorporated,

resulting for each coupling in a minimum three-step GFT NMR phase cycle (two steps for the cosine-modulated and one for the sine-modulated data set). Hence, for each mirrored sampled coupling, the minimal measurement time is increased by a factor of 1.5. In practice, however, it is worthwhile to also acquire the sine-modulated data set twice, so that the same signal-to-noise (S/N) ratios are obtained for the cosine- and sine-modulated data sets.

3. Methods

The extended formalism introduced above enables one to design *J*-GFT NMR experiments for accurate measurement of mutually correlated nuclear spin−spin couplings, in particular RDCs. Here we exemplify the new approach by implementing "*J*-GFT (6,2)D (HA−CA−CO)−N−HN", where each dash represents one of the measured one-bond spin−spin couplings, while for nuclei in parentheses the chemical shifts are, as usual, not measured. Hence, four mutually correlated one-bond couplings, namely, $^{13}C^{\alpha}-^{1}H^{\alpha}$ ($^{1}K_{C^{\alpha}H^{\alpha}}$), $^{13}C^{\alpha}-^{13}C'$ ($^{1}K_{C^{\alpha}C'}$), $^{15}N-^{13}C'$ ($^{1}K_{NC'}$), and $^{15}N-^{1}H^{N}$ ($^{1}K_{NH}$) spin−spin couplings, are measured in conjunction with ^{15}N and $^{1}H^{N}$ chemical shifts.

3.1. Implementation of *J*-GFT (6,2)D (HA−CA−CO)−N−HN. Using the rf pulse modules of Figure 3, constant-time (ct) *J*-GFT (6,2)D (HA−CA−CO)−N−HN was implemented (Figure 4). Except for ^{15}N, shifts are refocused during ct delays and only spin−spin couplings evolve in the indirect dimension. It is pivotal that the use of ct evolution ensures that signals do not broaden in the GFT dimension whenever multiple NMR parameters are jointly measured.[4] For the present implementation, backbone ^{15}N shifts are detected phase-sensitively, and multiplet splittings in the "basic spectra" [4] encode the four nuclear spin−spin couplings $^{13}C^{\alpha}-^{1}H^{\alpha}$, $^{13}C^{\alpha}-^{13}C'$, $^{15}N-^{13}C'$, and $^{15}N-^{1}H^{N}$ (Figure 5). Furthermore, encoded are (i) $^{13}C^{\alpha}-^{13}C'$, $^{15}N-^{13}C'$, and $^{15}N-^{1}H^{N}$ couplings and ^{15}N shifts in first-order central peak spectra, (ii) $^{15}N-^{13}C'$ and $^{15}N-^{1}H^{N}$ couplings and ^{15}N shifts in second-order central peak spectra, (iii) $^{15}N-^{1}H^{N}$ couplings and ^{15}N shifts in third-order central peak spectra, and (iv) ^{15}N shifts in fourth-order central peak spectra. Hence, a total of 31 2D planes constitute the (6,2)D (HA−CA−CO)−N−HN experiment, and the couplings are obtained from a least-squares fit to linear combinations of couplings. Specifically, $^{15}N-^{1}H^{N}$, $^{15}N-^{13}C'$, $^{13}C^{\alpha}-^{13}C'$, and $^{13}C^{\alpha}-^{1}H^{\alpha}$ couplings are detected, respectively, in 30, 28, 24, and 16 sub-spectra (Figure 5). Unambiguous grouping of multiplet components in the case of ^{15}N,$^{1}H^{N}$ shift degeneracy can be accomplished by "central peak detection", as it was introduced in reduced-dimensionality NMR spectroscopy.[6,32,33]

Unlike in IPAP[25] and other spin-state-filtered experiments,[26,27] modulations are achieved exclusively within the ct delays, so that line broadening arising from measuring multiple RDCs simultaneously and cancellation artifacts due to differential relaxation are avoided. Moreover, measurement of $^{1}K_{C^{\alpha}H^{\alpha}}$ during the $^{13}C^{\alpha}-^{13}C'$ transfer with transverse $^{13}C^{\alpha}$-polarization ensures that sensitivity losses due to $^{1}H^{\alpha}-^{1}H$ RDCs are minimized (adiabatic decoupling of aliphatic ^{1}H during signal detection could be employed to further enhance sensitivity[37]). For acquisition of the basic spectra, the delay τ_1 (Figure 4) was set to $\sim 3/2\ K^{ave}_{C^{\alpha}C'}$ (~27 ms) in order (i) to enable a maximum evolution time of 25 ms and (ii) to largely re-focus the passive $^{13}C^{\alpha}-^{13}C^{\beta}$ coupling ($^{1}J_{C^{\alpha}C^{\beta}} \approx 35$ Hz). For large proteins, one would evidently reduce τ_1 in order to avoid unacceptable losses in sensitivity. Then, the $^{1}K_{C^{\alpha}H^{\alpha}}$ coupling evolution has to be scaled down to retain the $^{13}C^{\alpha}-^{13}C'$ polarization transfer delay period of ~9 ms, and passive $^{13}C^{\alpha}-^{13}C^{\beta}$ couplings could be adiabatically decoupled.

Mirrored time domain sampling was implemented for the three largest one-bond couplings ($^{1}K_{NH}$, $^{1}K_{C^{\alpha}H^{\alpha}}$, and $^{1}K_{C^{\alpha}C'}$) (Figure 3b). The required transformation matrix, $\mathbf{G}^{mirrored}$, is provided as Supporting Information. Such mirrored time domain sampling doubles the minimal number of transients for each coupling, provided that the sine-modulated data set is also recorded twice (see section 2.3). Hence, the increase is 8-fold if three couplings are subject to mirrored sampling. With a single transient and a relaxation delay of 1.0 s between transients, the minimal measurement times are then ~6 h and ~45 min at 750 MHz ^{1}H resonance frequency, respectively, for mirrored and non-mirrored data acquisition of *J*-GFT (6,2)D (HA−CA−CO)−N−HN.

3.2. NMR Data Collection, Processing, and Analysis. The (6,2)D (HA−CA−CO)−N−HN experiment was implemented with a ~1 mM $^{13}C/^{15}N$ doubly labeled solution of unaligned protein Z-domain[38] ($M_r \approx 8$ kDa). RDCs were extracted from such an experiment recorded for a ~0.5 mM solution aligned with Pf1 phages[39] and characterized by a 25 Hz splitting of the $^{2}H_2O$ line. Both experiments were performed at 25 °C, once each on VARIAN INOVA 600 and 750 spectrometers equipped, respectively, with cryogenic and conventional triple-resonance probes. The acquisition parameters for the experiments are given in Table 1. To ensure identical rf pulse duty cycle, central peak spectra were acquired with the same rf pulse scheme by successively omitting coupling evolutions (Figure 4). (6,2)D (HA−CA−CO)−N−HN was recorded *with* and *without* mirrored time domain sampling of $^{1}K_{NH}$, $^{1}K_{C^{\alpha}H^{\alpha}}$, and $^{1}K_{C^{\alpha}C'}$ by acquiring 50 complex points along the indirect dimension ($t_{1max} = 25$ ms) in such a manner that the same acquisition time of 24 h was reached for the two experiments (including the recording of all central peak sub-spectra). Hence, for the non-mirrored data acquisition, 32 transients were acquired per increment, while 4 transients were acquired for the experiment recorded with mirrored sampling of three couplings. Moreover, $^{1}K_{C^{\alpha}H^{\alpha}}$ evolution was scaled to 1/3 in the experiment recorded without mirrored sampling of *J*-evolution in order to exemplify how to retain a $^{13}C^{\alpha}-^{13}C'$ transfer delay period of 8.8 ms ($\sim 1/2\ K^{ave}_{C^{\alpha}C'}$; note that adiabatic decoupling of $^{13}C^{\alpha}-^{13}C^{\beta}$ couplings could be employed during the transfer to enhance sensitivity[2]). The time domain data were processed using the G-matrices provided as Supporting Information and extended in both the dimensions by zero-filling prior to Fourier transformation (no linear prediction was employed). To assess the accuracy of RDCs obtained from (6,2)D (HA−CA−CO)−N−HN, the following conventional experiments were acquired within a total measurement time of 42 h (Table 1):[40] IPAP 2D [$^{15}N-^{1}H$] HSQC ($t_{1max} = 64$ ms), ω_1-^{15}N,$^{13}C'$-coupled 2D [^{15}N,^{1}H] HSQC ($t_{1max} = 250$ ms), ω_1-$^{13}C^{\alpha}$,$^{13}C'$-coupled 3D HNNCO ($t_{1max} = 33$ ms), and ct ω_1-$^{13}C^{\alpha}$,$^{1}H^{\alpha}$-coupled 3D HNN(CO)CA ($t_{1max} = 26$ ms). RDCs from the ω_1-coupled experiments were extracted from the peak splitting along ω_1. All spectra were processed using the program PROSA[41] and analyzed using the program XEASY.[42]

(32) (a) Szyperski, T.; Wider, G.; Bushweller, J. H.; Wüthrich, K. *J. Am. Chem. Soc.* **1993**, *115*, 9307−9308. (b) Brutscher, B.; Simorre, J. P.; Caffrey, M. S.; Marion, D. *J. Magn. Reson. Ser. B* **1994**, *105*, 77−82. (c) Szyperski, T.; Pellecchia, M.; Wüthrich, K. *J. Magn. Reson. Ser. B* **1994**, *105*, 188−191. (d) Szyperski, T.; Braun, D.; Banecki, B.; Wüthrich, K. *J. Am. Chem. Soc.* **1996**, *118*, 8146−8147. (e) Löhr, F.; Rüterjans, H. *J. Biomol. NMR* **1995**, *6*, 189−197. (f) Szyperski, T.; Banecki, B.; Braun, D.; Glaser, R. W. *J. Biomol. NMR* **1998**, *11*, 387−405. (g) Ding, K. Y.; Gronenborn, A. M. *J. Magn. Reson.* **2002**, *156*, 262−268.

(33) Szyperski, T.; Braun, D.; Fernandez, C.; Bartels, C.; Wüthrich, K. *J. Magn. Reson. Ser. B* **1995**, *108*, 197−203.

(34) Shaka, A. J. *Chem. Phys. Lett.* **1985**, *120*, 201−205.

(35) Kay, L. E.; Keifer, P.; Saarinen, T. *J. Am. Chem. Soc.* **1992**, *114*, 10663−10665.

(36) Jain, N. U.; Schroeder, N.; Prestegard, J. H. *J. Mol. Biol.* **2003**, *328*, 451−462.

(37) Vander Kooi, C. W.; Kupce, E.; Zuiderweg, E. R. P.; Pellecchia, M. *J. Biomol. NMR* **1999**, *15*, 335−338.

(38) (a) Tashiro, M.; Tejero, R.; Zimmerman, D. E.; Celda, B.; Nilsson, B.; Montelione, G. T. *J. Mol. Biol.* **1997**, *272*, 573−590. (b) Zheng, D.; Huang, Y. J.; Moseley, H. N. B.; Xiao, R.; Aramini, J.; Swapna, G. V. T.; Montelione, G. T. *Protein Sci.* **2003**, *12*, 1232−1246. (c) Zheng, D. Y.; Aramini, J. M.; Montelione, G. T. *Protein Sci.* **2004**, *13*, 549−554.

(39) Hansen, M. R.; Mueller, L.; Pardi, A. *Nat. Struct. Biol.* **1998**, *5*, 1065−1074.

(40) Bax, A.; Kontaxis, G.; Tjandra, N. *Methods Enzymol.* **2001**, *339*, 127−174.

(41) Güntert, P.; Dotsch, V.; Wider, G.; Wüthrich, K. *J. Biomol. NMR* **1992**, *2*, 619−629.

(42) Bartels, C.; Xia, T. H.; Billeter, M.; Güntert, P.; Wüthrich, K. *J. Biomol. NMR* **1995**, *6*, 1−10.

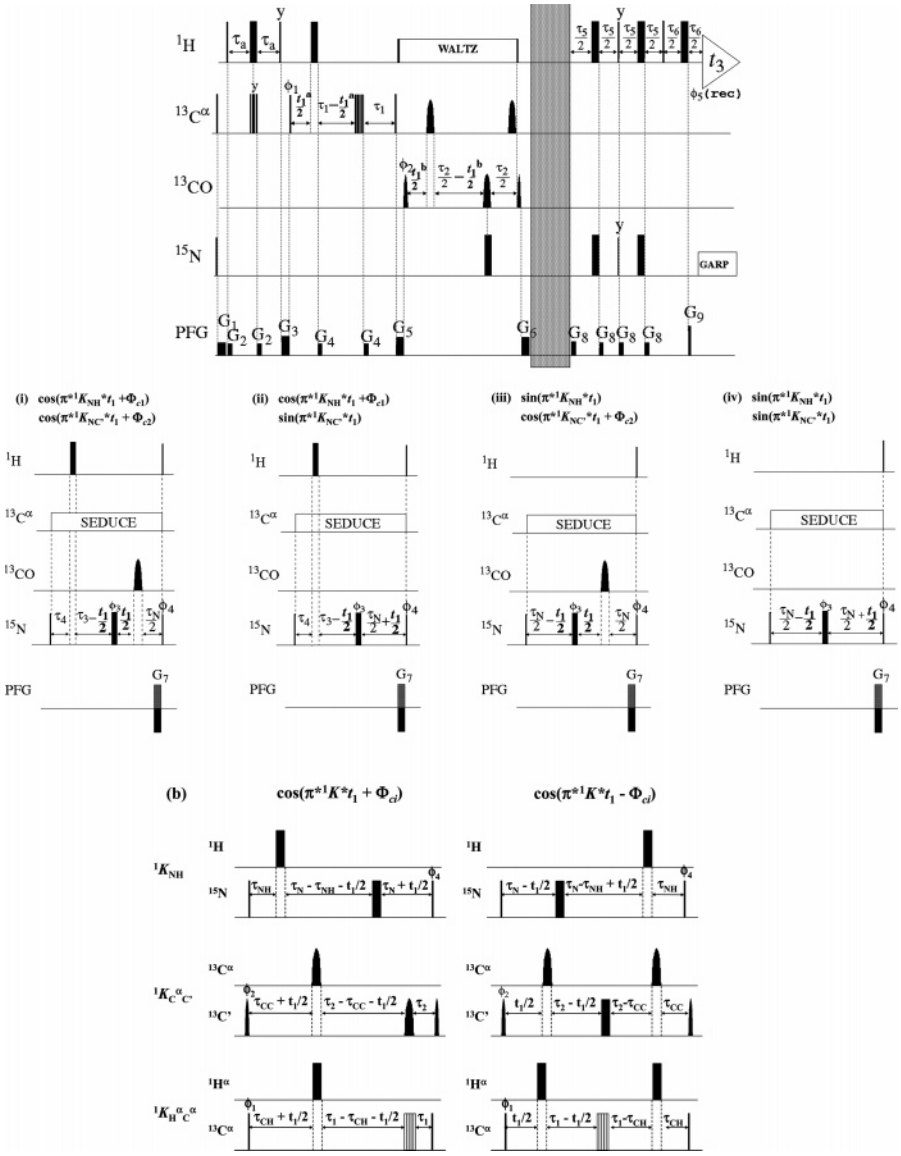

Figure 4. (a) Radio frequency pulse scheme of *J*-GFT (6,2)D (HA−CA−CO)−N−HN. Rectangular 90° and 180° pulses are indicated by thin and thick vertical bars, respectively, and phases are indicated above the pulses. Where no rf phase is marked, the pulse is applied along *x*. The shaded segment is expanded below the scheme according to the cosine and sine modulations that shall be accomplished (see below). The high-power 90° pulse lengths were 6.4 μs for ^{1}H, 15.0 μs for ^{13}C, and 44 μs for ^{15}N (^{1}H resonance frequency, 750 MHz). The ^{15}N rf carrier is set to 120.9 ppm. The ^{13}C carrier is set to 56 ppm initially and shifted to 176 ppm before the first pulse on ^{13}C′. Pulses on ^{13}C prior to $t_1{}^a$ are applied at high power, and ^{13}C coupling during the ^{1}H−^{13}C$^\alpha$ INEPT[1] is achieved using a ($90_x-180_y-90_x$) composite pulse. Subsequent 90° and 180° pulse lengths of ^{13}C$^\alpha$ are adjusted to 51.5 and 46 μs (^{1}H resonance frequency, 750 MHz), respectively, to minimize perturbation of the ^{13}C′ spins. A six-pulse composite sequence[34] is employed to simultaneously invert/refocus ^{13}C$^\alpha$/^{13}C′ magnetization during ^{13}C$^\alpha$−^{13}C′ polarization transfer and is represented by a group of six vertical bars. The width of the 90° SEDUCE pulses[1] applied to the ^{13}C′ pulse is 200 μs, and the corresponding 180° pulses are applied with the same power. WALTZ16[1] is employed to decouple ^{1}H (rf field strength, 7.5 kHz) during the heteronuclear magnetization transfers. GARP1[1] is used to decouple ^{15}N during acquisition (rf = 1.0 kHz). The off-resonance SEDUCE sequence[1] is used for decoupling of ^{13}C$^\alpha$ during the ^{15}N chemical shift evolution period. The ^{1}H rf carrier is placed at the position of the solvent line at 4.78 ppm. The duration and strengths of the pulsed *z*-field gradients (PFGs) are as follow: G1, 1 ms, 24 G/cm; G2, 100 μs, 8 G/cm; G3, 1 ms, 20 G/cm; G4, 500 μs, 8 G/cm; G5, 1.0 ms, 20 G/cm; G6, 1.0 ms, 20 G/cm; G7, 1.25 ms, 30 G/cm; G8, 500 μs, 8 G/cm; and G9, 125 μs, 29.5 G/cm. All PFG pulses are of rectangular shape. The delays are τ_a = 1.7 ms, τ_1 = 4.5 ms [τ_1 = 14 ms for detection $^1K(^1H^\alpha-^{13}C^\alpha)$ in basic spectra], τ_2 = 24.0 ms, t_3 = 13.6 ms, τ_4 = 2.7 ms, τ_5 = 4.6 ms, τ_6 = 1.0 ms, τ_N = 30 ms. Phase cycling: $\phi_1 = 2(x),2(-x)$; $\phi_2 = x,-x$; $\phi_3 = 4(x),4(-x)$; $\phi_4 = x$; ϕ_5(receiver) = $x,-x,-x,x$. A sensitivity enhancement scheme[35] is employed; i.e., the sign of G7 is inverted in concert with a 180° shift of ϕ_4. Quadrature detection of $t_1(^{15}N)$ is achieved by gradient selection of coherences using G7. All scaling factors are set to 1.0 for small and medium-sized proteins, while $\kappa_1 = 0.33$ for large proteins. To implement a CE-TROSY[36] version, $^1K_{NH}$ coupling evolution can be scaled with different values of κ_2 (Figure 3), which allows one to extract $^1K_{NH}$ from a change in multiplet component positions with varying κ_2. The required cosine and sine modulations are detected as follows: $^1K_{C^\alpha H^\alpha}$, cosine modulation with $t_1{}^a/2.0 = \kappa_1{*}t_1/2.0 + 1.7$ ms, sine modulation with $t_1{}^a/2.0 = \kappa_2{*}t_1/2.0$; $^1K_{C^\alpha C'}$, cosine modulation with $t_1{}^b/2.0 = \kappa_1{*}t_1/2.0 + 4.5$ ms, sine modulation with $t_1{}^b/2.0 = \kappa_2{*}t_1/2.0$; $^1K_{NH}/^1K_{NC'}$ ($\Phi_{ci} = \pi/2{*}(K_i - K_i{}^{ave})/K_i{}^{ave}$) ($K_i = {}^1K_{NH}, {}^1K_{NC'}$), cosine/cosine modulation as in inset (i), cosine/sine modulation as in inset (ii), sine/cosine modulation as in inset (iii), and sine/sine modulation as in inset (iv). Central peak spectra are acquired by successively omitting the coupling evolution of $^1K_{C^\alpha H^\alpha}$, $^1K_{C^\alpha C'}$, $^1K_{NC'}$, and $^1K_{NH}$. (b) Radio frequency pulse scheme modules incorporated into the scheme in (a) for mirrored sampling of time domain data for the evolution of $^1K_{NH}$, $^1K_{C^\alpha H^\alpha}$, and $^1K_{C^\alpha C'}$. Rectangular 90° and 180° pulses are indicated by thin and thick vertical bars, respectively. For each of the three couplings, four transients are independently acquired: one for each of the cosine modulations shown above and two for the sine modulations to ensure that the same signal-to-noise ratios are present in cosine- and sine-modulated data sets. Delays τ_1, τ_2, and τ_N and phases ϕ_1, ϕ_2, and ϕ_4 are as defined in (a), and other delays are τ_{NH} = 2.7 ms, τ_{CC} = 4.4 ms, and τ_{CH} = 1.7 ms.

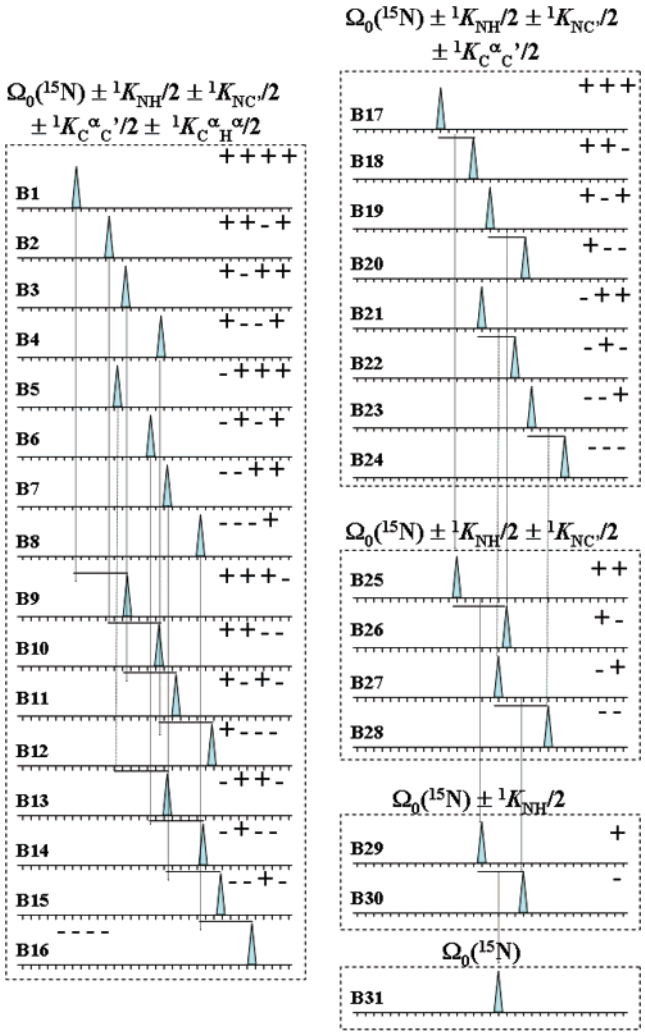

Figure 5. Peak pattern observed in *J*-GFT (6,2)D (HA−CA−CO)−N−HN. The sub-spectra are grouped into basic (B1−B16), first- (B17−B24), second- (B25−B28), and third-order (B29−B30) central peaks. The fourth-order central peak (B31) is a peak in 2D [^{15}N,^{1}H] HSQC. The linear combinations of couplings are indicated on top of each set and by the symbols "+/−" in the individual sub-spectra (for example, ++++ in B1 denotes $\Omega_0(^{15}N) + {}^1K_{NH} + {}^1K_{NC'} + {}^1K_{C^\alpha C'} + {}^1K_{C^\alpha H^\alpha}$). The dotted lines shown in B1−B16 indicate the respective peak pairs yielding ${}^1K_{C^\alpha H^\alpha}$, and those in B17−B30 indicate the position of peaks in the lower order central peak sub-spectra with respect to the corresponding higher order sub-spectra. The dark horizontal lines indicate the peak pair for a given splitting.

4. Results and Discussion

The theory of *J*-GFT NMR described in sections 2.1 and 2.2 paves the way to accurately measure groups of mutually correlated RDCs by use of two distinctly different approaches for dealing with spin-system-specific phase shifts of cosine-modulated signal components. First, a phase correction can be applied for each multiplet so that dispersive signal contributions are eliminated for the components of this multiplet. Second, mirrored sampling in the time domain can be employed to eliminate dispersive components for all signals. The two approaches are described in the following for data recorded for aligned 8 kDa protein Z-domain.[38] Subsequently, the RDCs derived from the data sets acquired *with* mirrored sampling were used to assess accuracy and precision of *J*-GFT NMR-derived couplings by comparison with RDCs extracted from conventional experiments.

4.1. Spin-System-Specific Phase Correction. In the sampling-limited data acquisition regime,[3] it is desirable to perform a *J*-GFT NMR experiment with a single transient per free induction decay and without resorting to mirrored time domain sampling (which increases the minimal measurement time at least by a factor of 1.5). Then, phase shifts of the cosine-modulated signal components introduce dispersive contributions into the line-shapes (Figures 2b and 6), which shift peak maxima. As an example, we demonstrate here the (iterative) employment of eq 9 for phasing of all components of a given multiplet in order to extract more accurate couplings from the first-order central peak spectrum of (6,2)D (HA−CA−CO)−N−HN. For a given spin system, the couplings are first measured in spectra processed without a phase correction. The couplings obtained in this way are used to calculate the phase matrix, and phase-corrected sub-spectra can be obtained from which more accurate couplings are derived. The resulting couplings are identical to those extracted from data sets acquired with mirrored sampling (see section 4.2), indicating that a single iteration is sufficient. Although being in principle straightforward and amenable to automated data analysis, this approach is, however, limited in cases of (partial) peak overlap. This is because the phase correction is *spin-system-specific*, so dispersive components of near-by peaks likely remain.

4.2. Mirrored Time Domain Sampling. Figure 7 shows the experimentally observed peak pattern in the (6,2)D (HA−CA−CO)−N−HN sub-spectra which were recorded for aligned and non-aligned 8 kDa protein Z-domain with use of mirrored time domain sampling for the evolution of ${}^1K_{NH}$, ${}^1K_{C^\alpha H^\alpha}$, and ${}^1K_{C^\alpha C'}$. As a result, dispersive signal components are eliminated. Moreover, residual "quadrature images" resulting from the slightly different amplitudes of cosine- and sine-modulated signals (eq 14; Figure 2c) are apparently below the detection limit.[43] Correlated ^{15}N−^{1}H^N, ^{13}C′−^{15}N, ^{13}C$^\alpha$−^{13}C′, and ^{1}H$^\alpha$−^{13}C$^\alpha$ RDCs were measured for 51 out of 54 spin systems (prolyl and the N-terminal residues do not possess detectable amide protons), which corresponds to a yield of ∼90%. For the remaining spin systems, accurate measurement of RDCs was impeded by exchange-broadened lines. Plots of RDCs versus the polypeptide sequence are shown in Figures S2 of the Supporting Information.

4.3. Precision and Accuracy of RDCs from *J*-GFT NMR. To assess the precision of RDC measurements using (6,2)D (HA−CA−CO)−N−HN, the experiment was conducted twice at two different field strengths, corresponding to ^{1}H resonance frequencies of 600 and 750 MHz (Table 1). Analysis of the two experiments (named "600 MHz" and "750 MHz" in the following) yielded two statistically independent sets of ^{15}N−^{1}H^N, ^{13}C′−^{15}N, ^{13}C$^\alpha$−^{13}C′, and ^{1}H$^\alpha$−^{13}C$^\alpha$ RDCs (Table S2, Supporting Information). Comparison of the two sets revealed root-mean-square deviation (rmsd) values which are smaller than 1 Hz for all four types of RDCs (Figure 8a). Notably, cross-correlation effects and variations of RDCs due to the difference in field strengths can be neglected.[44] As was shown for ct GFT

(43) Typically, one has that $\Phi_{ci} = \pi/2*(K_i - K_i^{ave})/K_i^{ave} < 30°$ for all spin−spin couplings. This was also observed for protein Z-domain in the present study (Table S2). In rare cases with $\Phi_{ci} > 30°$, or when *J*-GFT NMR spectra are recorded with very high S/N ratios, the imbalance of cosine- and sine-modulated signals (eq 14) may give rise to quadrature artifacts (Figure 2c). Such minor artifacts can then be suppressed by up-scaling of the cosine-modulated signals by $1/\cos(\Phi_{ci})$ for each *i*. However, since the phases Φ_{ci} are spin-system-specific, such scaling has to be performed for each multiplet separately.

(44) (a) Tjandra, N.; Bax, A. *J. Magn. Reson.* **1997**, *124*, 512−515. (b) Yang, D.; Tolman, J. R.; Goto, N. K.; Kay, L. E. *J. Biomol. NMR* **1998**, *12*, 325−332. (c) Feher, K.; Berger, S. *J. Magn. Reson.* **2004**, *170*, 191−198.

Table 1. Acquisition Parameters of NMR Experiments

experiment[a]	indirect dimension: t_{max} (ms); complex points; digital resolution (Hz/point)[b]	measuremen time (h)	S/N[c]	line width[c] (ω_1, Hz)
(6,2)D (HA−CA−CO)−N−HN[d]	ω_1: 25.0; 50; 0.48	24.0	7.6 ± 2.7	33 ± 3.7
IPAP 2D [^{15}N−^{1}H] HSQC[e]	ω_1(^{15}N): 64.0; 128; 0.48	2.5	21 ± 5.3	16 ± 1.7
ω_1-^{15}N,^{13}C′-coupled 2D [^{15}N,^{1}H] HSQC[e]	ω_1(^{15}N): 256.0; 512; 0.48	5.5	43 ± 9.3	7.1 ± 0.9
ω_1-^{13}C$^{\alpha}$,^{13}C′-coupled 3D HNNCO[e]	ω_1(^{13}C): 33.0; 64; 2.0 ω_2 (^{15}N): 16.0; 32; 31.2	10.5	62 ± 11.1	24 ± 0.9
ct ω_1-^{13}C$^{\alpha}$,^{1}H$^{\alpha}$-coupled 3D HNN(CO)CA[e]	ω_1(^{13}C): 26.0; 128; 4.8 ω_2 (^{15}N): 16.0; 32; 31.2	23.5	20 ± 5.1	33 ± 1.9

[a] All experiments were recorded with identical parameters for aligned and non-aligned protein Z-domain. [b] Direct dimension, ω_2(^{1}H)/ω_3(^{1}H): 64; 512; 4. Relaxation delay between transients, 1.1 s. [c] Average signal-to-noise (S/N) ratios and line widths are for data recorded at 750 MHz for aligned protein Z-domain. [d] Recorded at ^{1}H resonance frequencies of 600 and 750 MHz. Includes 10 min to record a 2D [^{15}N,^{1}H] HSQC, i.e., a fourth-order central peak spectrum, with two scans per FID (t_{max}(^{15}N) = 64 ms). Other spectra were acquired with four transients per free induction decay. [e] Recorded at 750 MHz ^{1}H resonance frequency.

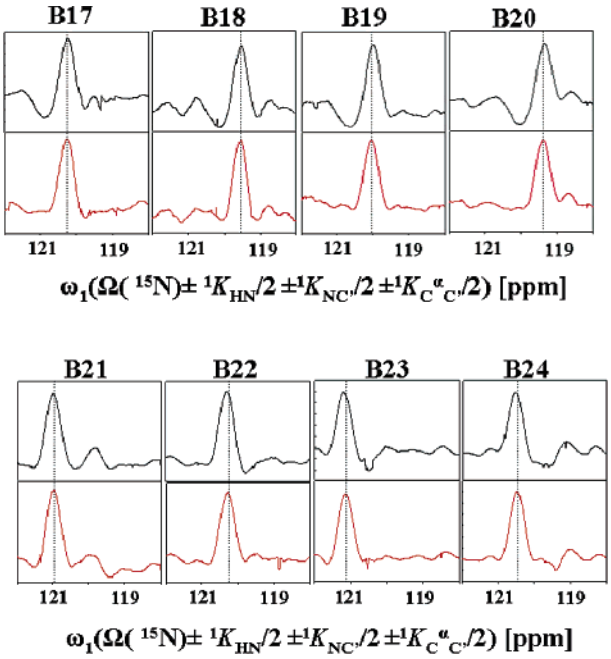

Figure 6. Illustration of spin-system-specific phase correction of *J*-GFT sub-spectra by computing a phase matrix from approximate RDCs and by use of eq 9. Cross sections were taken along $\omega_1[\Omega(^{15}N) \pm {}^{1}K_{NH}/2 \pm {}^{1}K_{NC'}/2 \pm {}^{1}K_{C^{\alpha}C'}/2]$ from the (6,2)D (HA−CA−CO)−N−HN (Figure 4) first-order central peak sub-spectra B17−B24 (for the definition of the linear combinations of couplings that are observed, see Figure 5), recorded for aligned 8 kDa protein Z-domain. Signals arise from the spin system ^{13}C$^{\alpha}$-(Lys 49)−^{13}C′(Lys 49)−^{15}N (Lys 50). The cross sections shown in black (top) are obtained without phase correction, and the line shape distortions are apparent. The following couplings are obtained from these signals: $^{1}D_{NH} = -22$ Hz, $^{1}D_{NC'} = 3.0$ Hz, and $^{1}D_{C^{\alpha}C'} = 0.0$ Hz. In turn, those were taken to calculate the phase matrix in eq 9, giving the phase-corrected cross sections shown in red (bottom). The phase-corrected signals yield more accurate values for the RDCs: $^{1}D_{NH} = -24.4$ Hz, $^{1}D_{NC'} = 3.2$ Hz, and $^{1}D_{C^{\alpha}C'} = 0.0$ Hz.

NMR,[4,5b] the high precision arises from the fact that the RDC values are derived from over-determined systems of equations: $n^{eq} = 30$, 28, 24, and 16 signals serve to derive, respectively, the ^{15}N−^{1}H^{N} (rmsd = 0.90 Hz), ^{15}N−^{13}C′ (0.85 Hz), ^{13}C$^{\alpha}$−^{13}C′ (0.80 Hz), and ^{13}C$^{\alpha}$−^{1}H$^{\alpha}$ (0.75 Hz) couplings (Figure 8).

Considering the equation rmsd = $(\sigma^2(600\text{ MHz}) + \sigma^2(750\text{ MHz}))^{1/2} = (2^{1/2})\sigma^{ave}$, where $\sigma^{ave} = {}^{1}/_{2}\,[\sigma(600\text{ MHz}) + \sigma(750\text{ MHz})] \approx \sigma(600\text{ MHz}) \approx \sigma(750\text{ MHz})$, one obtains that σ^{ave}-(*J*-GFT) ≈ 0.5 Hz for all four types of couplings (Table 2). Such high precision is evidently well suitable for most conceivable applications in NMR-based structural biology.[15]

To assess the accuracy of RDCs obtained from ct *J*-GFT (6,2)D (HA−CA−CO)−N−HN, the couplings were also measured by use of well-established conventional NMR experiments performed at 750 MHz ^{1}H resonance frequency (Table 1). Root-mean-square deviation values between 0.75 and 1.6 Hz were obtained for pairs of couplings (Figure 8b), and a least-squares fit of *J*-GFT NMR-based and conventionally determined RDCs to a linear function reveals that slope and intercepts are, respectively, 1 and 0 within the experimental error (Table 3). Hence, no systematic errors could be detected, demonstrating comparable accuracy between ct *J*-GFT NMR-based and conventional measurements.

Since systematic errors are negligible for both GFT NMR-based and conventional measurement of RDCs, one can compare the relative precision of RDC measurements for each type of coupling when considering that rmsd = $((\sigma^2(\text{GFT, 750 MHz}) + \sigma^2(\text{conventional, 750 MHz}))^{1/2}$. Since σ(*J*-GFT, 750 MHz) ≈ σ^{ave}(*J*-GFT) is known, this equation enables one to calculate σ(conventional, 750 MHz) (Table 2).

In GFT NMR, standard deviations are expected to scale according[4,5a] to $1/\sqrt{n^{eq}}$, where n^{eq} represents the number of equations used to calculate a given type of NMR parameter. In (6,2)D (HA−CA−CO)−N−HN, the ^{15}N−^{1}H^{N}, ^{15}N−^{13}C′, ^{13}C$^{\alpha}$−^{13}C′, and ^{13}C$^{\alpha}$−^{1}H$^{\alpha}$ couplings are encoded in linear combinations measured in, respectively, 30, 28, 24, and 16 sub-spectra (Figure 5), while two sub-spectra are acquired in the conventional experiments. Hence, the standard deviations for a given type of coupling in (6,2)D (HA−CA−CO)−N−HN relative to the conventional experiment are expected to scale with $(1/\sqrt{n^{eq}})/(1/\sqrt{2}) = 1/\sqrt{(n^{eq}/2)}$, that is, by $1/\sqrt{15} = 1/3.9$ for ^{15}N−^{1}H^{N}, $1/\sqrt{14} = 1/3.8$ for ^{15}N−^{13}C′, $1/\sqrt{12} = 1/3.5$ for ^{13}C$^{\alpha}$−^{13}C′, and $1/\sqrt{8} = 1/2.8$ for ^{13}C$^{\alpha}$ −^{1}H$^{\alpha}$ couplings. Moreover, standard deviations scale in both *J*-GFT and conventional NMR experiments with $\Delta\nu$, where $\Delta\nu$ represents the line width,[5a,29] so that σ(conventional)/σ(*J*-GFT) scales with $\sqrt{(n^{eq}/2)}[\Delta\nu(\text{conventional})/\Delta\nu(J\text{-GFT})]$.

As a result, the precision of a $^{1}D_{NC'}$ measurement is about the same in (6,2)D (HA−CA−CO)−N−HN and ω_1-^{15}N,^{13}C′-coupled 2D [^{15}N,^{1}H] HSQC (Tables 1−3): about 4-fold narrower lines in ω_1-^{15}N,^{13}C′-coupled 2D [^{15}N,^{1}H] HSQC balance the over-determination in (6,2)D (HA−CA−CO)−N−HN. For the other types of couplings, the scaling of σ(*J*-GFT) with $1/\sqrt{(n^{eq}/2)}$ dominates, so that measurements in (6,2)D (HA−CA−CO)−N−HN are more precise when compared with the corresponding conventional experiments listed in Table 1. The largest gain in precision (about 3-fold) is registered for $^{1}D_{C^{\alpha}H^{\alpha}}$ since about the same line widths are observed in (6,2)D (HA−CA−CO)−N−HN and ct ω_1-^{13}C$^{\alpha}$,^{1}H$^{\alpha}$-coupled 3D HNN-

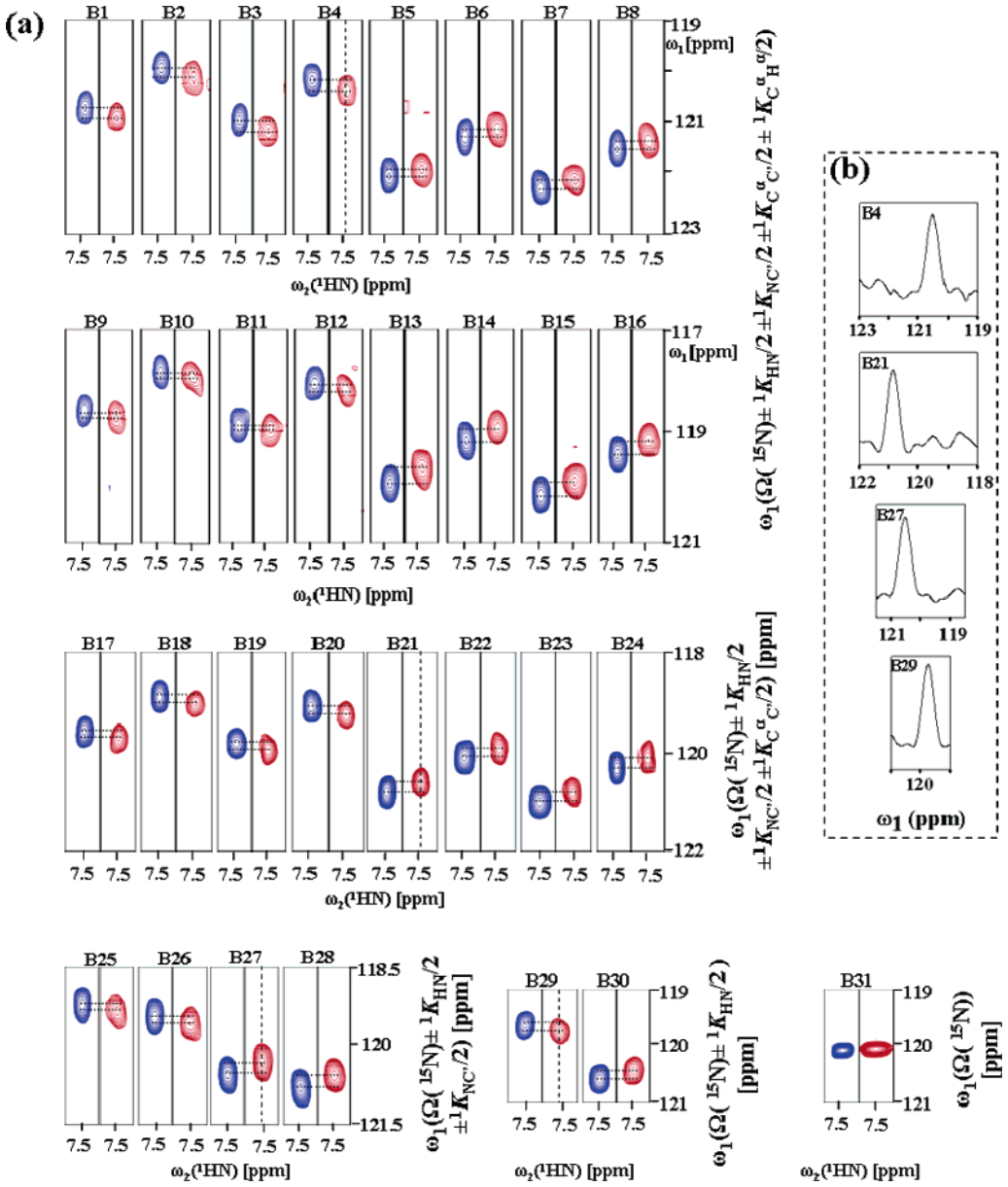

Figure 7. (a) Composite plot of $[\omega_1,\omega_2]$ strips taken along the GFT dimension of sub-spectra constituting a *J*-GFT (6,2)D (HA−CA−CO)−N−HN experiment, acquired at a ^{1}H resonance frequency of 750 MHz using mirrored time domain sampling for non-aligned (blue) and aligned (red) samples of protein Z-domain. Signals arise from the spin system $^1H^\alpha$(Lys 49)−$^{13}C^\alpha$(Lys 49)−$^{13}C'$(Lys 49)−^{15}N(Lys 50) and are detected on the amide proton of Lys 50. The linear combinations of chemical shifts and spin−spin couplings corresponding to the individual spectra are provided in Figure 5. The dotted horizontal lines indicate shifts in peak positions arising from linear combinations of RDCs: $^1D_{NH} = -24.4$ Hz, $^1D_{NC'} = 3.2$ Hz, $^1D_{C^\alpha C'} = 0.1$ Hz, and $^1D_{C^\alpha H^\alpha} = 9.8$ Hz. (b) Cross sections taken along ω_1 from sub-spectra B4, B21, B27, and B29 [indicated by dotted vertical lines in (a)], which show that purely absorptive line shapes are obtained due to mirrored time domain sampling.

(CO)CA. Considering that standard deviations of $^{13}C^\alpha-^1H^\alpha$ coupling measurements are typically significantly larger than 1 Hz,[44b,45] we conclude that *J*-GFT NMR spectroscopy provides a unique approach for measuring these couplings with unprecedented precision. This might well impact on the accuracy of RDC-refined NMR structures.[15]

5. Conclusions

Constant-time (ct) *J*-GFT NMR spectroscopy represents a promising novel approach for correlated measurement of several types of spin−spin couplings and chemical shifts according to spin system. High precision is accomplished since the couplings are derived from over-determined systems of equations. Joint measurement of one chemical shift and four spin−spin couplings is exemplified here by use of ct *J*-GFT (6,2)D (HA−CA−CO)−N−HN. The delays required for polarization transfer and evolution of the couplings can be used for chemical shift evolution of additional spins in order to increase spectral dispersion. Thus, one can devise congener experiments such as (7,2)D (HA−CA)−CO−N−HN or (7,3)D (HA−CA)−CO−N−HN, which may well be of value whenever severe $^{15}N-^1H$ chemical shift degeneracy is encountered.

(45) (a) Vuister, G. W.; Delaglio, F.; Bax, A. *J. Am. Chem. Soc.* **1992**, *114*, 9674−9675. (b) Zweckstetter, M.; Bax, A. *J. Am. Chem. Soc.* **2001**, *123*, 9490−9491.

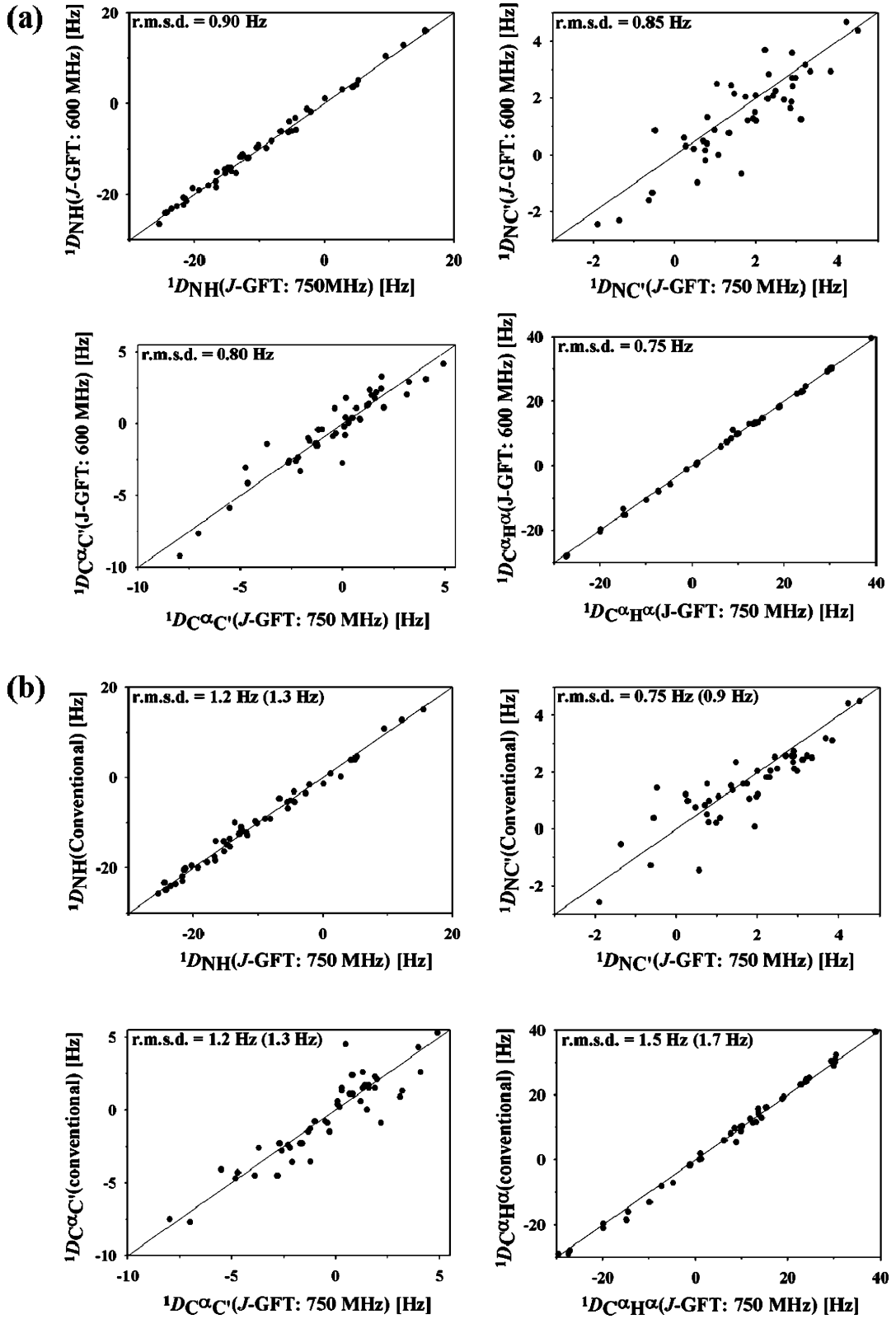

Figure 8. (a) Assessment of precision of RDC measurements in (6,2)D (HA−CA−CO)−N−HN. Comparison of RDCs measured for aligned protein Z-domain at a ^{1}H resonance frequency of 600 MHz (*y*-axis) versus RDCs obtained at a ^{1}H resonance frequency of 750 MHz (*x*-axis). (b) Assessment of accuracy of RDC measurements in (6,2)D (HA−CA−CO)−N−HN. Comparison of RDCs measured in conventional experiments at 750 MHz ^{1}H resonance frequency (*y*-axis) versus RDCs measured in (6,2)D (HA−CA−CO)−N−HN at 750 MHz ^{1}H resonance frequency (*x*-axis). Pairwise rmsd values are given in the upper left corners of the plots. For completeness, the corresponding rmsd values from comparing conventionally determined RDCs with 600 MHz *J*-GFT RDCs are given in parentheses.

Moreover, instead of an "out-and-stay"-type[1] implementation, as in *J*-GFT (6,2)D (HA−CA−CO)−N−HN, analogous "out-and-back" HN-detected *J*-GFT experiments appear to be the preferred choice for large and/or deuterated proteins. This is because the out-and-back polarization transfer allows one to incorporate TROSY[28,46] as well as longitudinal ^{1}H relaxation

Table 2. Standard Deviations (σ) of RDC Measurements.

RDC type	σ^{ave} (Hz)	
	J-GFT[a]	conventional[b]
$^1D_{NH}$	0.64	1.02
$^1D_{NC'}$	0.60	0.45
$^1D_{C^\alpha C'}$	0.56	1.06
$^1D_{C^\alpha H^\alpha}$	0.53	1.40

[a] Estimated using the relation rmsd $= (2^{1/2})\sigma^{ave}$(*J*-GFT) (rmsd values taken from figure 8a). [b] Estimated using the relation rmsd $= (\sigma^2$(GFT, 750 MHz) $+ \sigma^2$(conventional, 750 MHz))$^{1/2}$ (rmsd values taken from Figure 8b; see text).

Table 3. Statistics of RDC Measurements

RDC type	rmsd values[a] (Hz)		coefficients of linear regression[b]	
	GFT, 750 vs GFT, 600 MHz	GFT, 750 vs conventional, 750 MHz	*A*	*B* (Hz)
$^1D_{NH}$	0.90	1.2 (1.3)	0.98 ± 0.02	-0.22 ± 0.24
$^1D_{NC'}$	0.85	0.75 (0.90)	0.85 ± 0.07	0.06 ± 0.15
$^1D_{C^\alpha C'}$	0.80	1.2 (1.3)	0.96 ± 0.06	-0.15 ± 0.17
$^1D_{C^\alpha H^\alpha}$	0.75	1.5 (1.7)	1.03 ± 0.01	-0.55 ± 0.17

[a] Numbers from Figure 8. The numbers given in parentheses are GFT, 600 MHz vs conventional, 750 MHz. [b] RDCs from conventional NMR (y) and *J*-GFT NMR (x) data were fitted to $y = Ax + B$.

optimization[5b,47] for increasing sensitivity and/or enable more rapid data collection. For large proteins, CE-TROSY[36]-type variants promise accurate measurement of $^{15}N-^1H$ and $^{15}N-^{13}C'$ couplings. For example, due to the very high sensitivity of HNNCO-type experiments, *J*-L-GFT-CE-TROSY (4,2)D HN−N−(CO) appears to be a quite promising candidate for measuring such couplings in large deuterated proteins [alternatively, one might consider recording *J*-L-GFT-CE-TROSY (5,2)D HN−N−(CO-CA) or congeners]. Furthermore, measurement of the small one-bond $^{13}C'-^{15}N$ and $^{13}C^\alpha-^{13}C'$ couplings can be readily omitted in out-and-stay (6,2)D (HA−CA−CO)−N−HN. The resulting (4,2)D (HA−CACO)N−HN experiment exhibits 4-fold increased sensitivity and promises to be a valuable experiment to measure mutually correlated $^{15}N-^1H^N$ and $^{13}C^\alpha-^1H^\alpha$ couplings with high precision in medium to large proteins, or whenever sensitivity becomes a limiting constraint for data collection.

A key advantage of measuring RDCs in *J*-GFT NMR is attributed to the fact that the RDC values are grouped according to spin system, even if no sequential assignments are available. Therefore, we expect that such spectroscopy will be of value for rapid classification of protein fold families on the basis of statistical analysis of dipolar couplings. It has been shown that $^{15}N-^1H$ RDC probability density functions alone allow one to assess the novelty of the fold of a target protein,[22b] and an extension of this approach with several types of mutually correlated RDCs might well lead to increased reliability.

The use of RDCs for structure validation and refinement, as well as for identification of regular secondary structure elements of proteins in solution or when embedded in a membrane mimic, is obvious. For the high-throughput protein structure determination pipelines in structural genomics, an experiment such as (4,2)D (HA−CACO)N−HN appears to be an attractive choice. The two large $^{15}N-^1H$ and $^{13}C^\alpha-^1H^\alpha$ couplings are highly valuable for structure validation and refinement and are obtained for each (non-prolyl) residue, even when $^{15}N-^1H^N$ chemical shift degeneracy is encountered. This is of particular interest for homo-dimeric protein−protein complexes which represent significant challenges for high-throughput pipelines. In addition, we propose here to consider measurement of mutually correlated RDCs by use of *J*-GFT NMR as a complementary approach to assess variations of dynamics along the polypeptide chain in structural genomics. Differences between measured RDCs and values predicted on the basis of a three-dimensional structure reflect dipolar coupling averaging arising from internal motional modes.[21] Importantly, simultaneous fitting of both structural and dynamics parameters to an experimental constraint set consisting of NOE-derived distance constraints and RDC-derived orientational constraints might be quite well suited for establishing a first step toward high-throughput protein dynamics.

Finally, the extended *J*-GFT NMR formalism enables one to relax on constraints for the design of new GFT NMR experiments. For example, mirrored time domain sampling can be used whenever the realization of non-shifted sinusoidal modulations is not feasible. As such, the novel methodology presented here for implementing *J*-GFT NMR can be expected to have a broad impact on projection NMR spectroscopy in general.

Acknowledgment. This research is supported by the National Science Foundation (MCB 0416899 to T.S.) and the Protein Structure Initiative of the National Institutes of Health (U54 GM074958-01 and U54 GM075026-01). We thank Drs. G. Montelione and J. Aramini, Rutgers University, for providing samples of protein Z-domain, and Dr. J. Prestegard, University of Georgia, for stimulating discussions.

Supporting Information Available: Phase matrix for phase correction of (*N*,*N*−2)D GFT NMR spectra (see Figure 1); Table S1 with product operator terms for rf pulse modules used for *J*-GFT NMR (see Figure 3); alternative rf pulse modules for joint sampling of chemical shift and scalar coupling; G-matrix transformation of *J*-GFT (6,2)D (HA−CA−CO)−N−HN; Table S2 with RDC values obtained from *J*-GFT and conventional NMR; and Figure S1 with a plot of RDC values along the polypeptide chain for protein Z-domain. This material is available free of charge via the Internet at http://pubs.acs.org.

JA066586S

(46) Salzmann, M.; Wider, G.; Pervushin, K.; Senn, H.; Wüthrich, K. *J. Am. Chem. Soc.* **1999**, *121*, 844−848.
(47) Pervushin, K.; Vogeli, B.; Eletsky, A. *J. Am. Chem. Soc.* **2002**, *124*, 12898−12902.